



Evaluation of thiadiazine-based PET radioligands for imaging the AMPA receptor

Jiahui Chen^{a,b,1}, Wenqing Ran^{a,1}, Yiman Huang^{c,1}, Junjie Wei^{a,e}, Jian Rong^b, Huiyi Wei^a, Yinlong Li^b, Guocong Li^{a,e}, Zhen Chen^b, Lee Collier^b, Nehal H. Elghazawy^d, Wolfgang Sippl^d, Ahmed Haider^b, Kai Liao^a, Chenchen Dong^a, Ying Li^a, Hao Xu^{a,e}, Wenpeng He^{c,*}, Lu Wang^{a,e,**}, Steven H. Liang^{b,*}

^a Center of Cyclotron and PET Radiopharmaceuticals, Department of Nuclear Medicine and PET/CT-MRI center, The First Affiliated Hospital of Jinan University, Guangzhou 510630, China

^b Division of Nuclear Medicine and Molecular Imaging, Massachusetts General Hospital & Department of Radiology, Harvard Medical School, Boston, MA 02114, USA

^c Medical Center of Stomatology, The First Affiliated Hospital of Jinan University, Jinan University School of Stomatology, Guangzhou 510630, China

^d Institute of Pharmacy, Department of Medicinal Chemistry, Martin-Luther-University Halle-Wittenberg, W.-Langenbeck-Str. 4, 06120 Halle, Germany

^e Key Laboratory of Basic and Translational Research on Radiopharmaceuticals, The First Affiliated Hospital of Jinan University, Guangzhou 510630, China

ARTICLE INFO

Keywords:

AMPA receptors
Central nervous system (CNS)
Positron emission tomography
Positive allosteric modulator (PAM)
Fluorine 18 (¹⁸F)

ABSTRACT

As a subclass of ionotropic glutamate receptors (iGluRs), α -amino-3-hydroxyl-5-methyl-4-isoxazolepropionic acid (AMPA) receptors have been implicated in various neurological disorders and neurodegenerative diseases. To further our understanding of AMPA receptor-related disorders in the central nervous system (CNS), it is important to be able to image and quantify AMPA receptors in vivo. In this study, we identified a novel F-containing AMPA positive allosteric modulator (PAM) **6** as a potential lead compound. Molecular docking studies and CNS PET multi-parameter optimization (MPO) analysis were used to predict the absorption, distribution, metabolism, and excretion (ADME) characteristics of **6** as a PET probe. The resulting PET probe, [¹⁸F]**6** (code-name [¹⁸F]AMPA-2109), was successfully radiolabeled and demonstrated excellent blood-brain barrier (BBB) permeability and high brain uptake in rodents and non-human primates. However, [¹⁸F]**6** did not show substantial specific binding in the rodent or non-human primate brain. Further medicinal chemistry efforts are necessary to improve specific binding, and our work may serve as a starting point for the design of novel ¹⁸F-labeled AMPA receptor-targeted PET radioligands aimed for clinical translation.

1. Introduction

As a subtype of ionotropic glutamate receptors, α -amino-3-hydroxy-5-methyl-4-isoxazolepropionic acid (AMPA) receptors, mediate the rapid excitatory transmission of glutamate, which exert a vital role in signal transduction and neurodevelopment in the central nervous system (CNS) [1]. AMPA receptors are widely distributed in the brain, but mainly located in the hippocampus, outer cortex, olfactory area, lateral septum, basal ganglia and amygdala [2–4]. Recent studies have indicated that dynamic expression of AMPA receptors in the postsynaptic membrane may lead to prolonged inhibition of the neuronal pathway

which is oftentimes seen in disease processes such as schizophrenia, epilepsy, and Alzheimer's disease [5]. Therefore, targeting AMPA receptors may suggest high therapeutical consequence, therefore leading to numerous ongoing efforts in drug discovery.

Several antagonists targeting AMPA receptors have been developed in early drug discovery. Perampanel is the first highly selective, non-competitive AMPA receptor antagonist that is approved by U.S. Food and Drug Administration. However, probably attributed to wide distribution of receptors in multiple brain regions, AMPA receptor antagonists are often accompanied by adverse effects such as sedation and vertigo [6]. Recently, novel positive allosteric modulators (PAMs) of AMPA

* Corresponding authors.

** Corresponding author at: Center of Cyclotron and PET Radiopharmaceuticals, Department of Nuclear Medicine and PET/CT-MRI center, The First Affiliated Hospital of Jinan University, Guangzhou 510630, China.

E-mail addresses: a_bu1998@163.com (W. He), l_wang1009@jnu.edu.cn (L. Wang), steven.liang@emory.edu (S.H. Liang).

¹ These authors contributed equally to this work.

receptors have been developed, which represents a promising approach for not only drug discovery but also the companion imaging ligand development [7]. PAMs are bound to an allosteric pocket of the AMPA subunits, fine-tuning the function of AMPA receptors, and could potentially address the excitotoxic effect of agonists [6]. As such, the development of PAMs with high affinity has stimulated considerable interest in the field of medicinal discovery and drug discovery.

Positron emission tomography (PET) is a powerful non-invasive imaging technique capable of visualizing *in vivo* physiopathological processes, which provides a diagnostic and/or target engagement tool in drug discovery [8]. Imaging and quantification AMPA receptors in the CNS is critical to advancing our understanding of AMPA receptor-related disorders [9]. Currently, there are several AMPA receptor antagonist based PET tracers have been developed based on the Perampanel scaffold (Fig. 1A), including [^{11}C]perampanel [10], [^{11}C]1 [11], and our ligand [^{18}F]2 [12]. Although preliminary evaluation showed that all these tracers possessed high initial brain uptake, high specific binding *in vivo* remained a challenge. An ^{11}C -labeled PAM type PET tracer, [^{11}C]K-2 ([^{11}C]3) [13], was recently developed (Fig. 1B), which exhibited high binding affinity and specificity yet with rapid metabolism *in vivo*. Furthermore, the short half-life of C-11 ($t_{1/2} = 20.4$ min) restricted further clinical translation and application due to the need of an on-site cyclotron. Another PAM type tracer, [^{18}F]BPAM121 ([^{18}F]4) was reported to have a moderate uptake in mouse brain but could not be blocked in competition studies, which is not suitable for PET ligands [14]. So far, the development of ^{18}F -labeled AMPA receptor PET tracers based on allosteric modulators is still at the initial stage. Based on 4-cyclopropyl-7-(3-methoxyphenoxy)-3,4-dihydro-2H-benzo[e][1,2,4]thiadiazine 1,1-dioxide ($\text{EC}_{50} = 2$ nM) [15], we reported a novel ^{11}C -labeled PAM type tracer [^{11}C]AMPA-1905 ([^{11}C]5) which possessed good blood-brain barrier (BBB) permeability [16]. In this work, we took advantage of a similar scaffold, and identified a novel fluorinated PAM 6 as a lead compound from molecular docking studies and CNS permeability prediction by CNS PET multi-parameter optimization analysis. The binding affinity (Kd) of compound 6 was measured to be 0.35 μM . Additionally, Compound 6 was found in a functional study to increase AMPA-evoked response markedly by a factor of 15 with an EC_{50} of 0.90 μM [17]. Although the potency of PAM 6 is suboptimal for PET ligand development, we sought to profile the structural scaffold of this type and study the pharmacokinetics in the brain of difference species in order to

design new PET ligands. We utilized copper-mediated radiofluorination for the preparation of [^{18}F]6 (codename [^{18}F]AMPA-2109) and performed PET imaging in rodents and non-human primates (NHPs), demonstrating that radioligand [^{18}F]6 exhibited improved brain permeability for further optimization.

2. Results and discussion

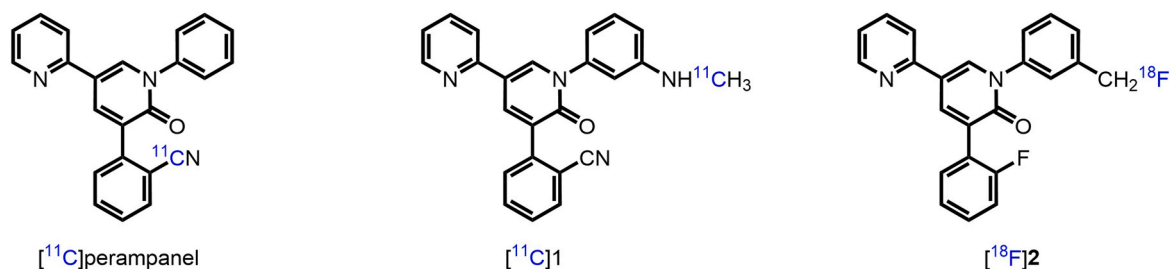
2.1. Molecular docking studies

To investigate the molecular interaction of compounds 5 and 6 in the GluA2-binding ligand domain (BLD) of AMPA receptors, the published AMPA receptor co-crystal x-ray structures (PDB ID: 4n07 and 5oew) were used as docking platform. As shown in Fig. 2, compounds 5 and 6 exhibited good interactions with GluA2-BLD residues. All possible interactions within 5 Å from compounds to surrounding residues were measured. The hydrogen bond was formed from the backbone Pro105 to nitrogen atom, respectively. Compound 6 formed two more Van der Waals interaction than compound 5 due to the presence of the 3'-methoxyphenoxy in compound 5. This group restricts the deflection of the molecular structure as well as the formation of Van der Waals interaction. However, an extra hydrogen bond was formed from the sulfonamide O atom of 5 to residue Ser242, and extra amide- π stacked was formed from 5 to Lys218, which implied a stronger interaction between 5 and GluA2-BLD (Fig. 2C & 2D). These results may provide a rationale of a decreasing binding affinity of compound 6 towards GluA2-BLD of AMPA receptors.

2.2. CNS PET multi-parameter optimization analysis

We utilized CNS multi-parameter optimization (CNS MPO) and CNS PET multi-parameter optimization (CNS PET MPO) to predict physicochemical properties and brain penetration of compounds 5 and 6 [18, 19]. ACD/Labs software (Toronto, Canada) was used to estimate all six fundamental physicochemical properties considered in candidates, including cLogP, cLogD, molecular weight (MW), topological polar surface area (tPSA), number of hydrogen bond donors (HBD), and ionization constant of the most basic center (pKa). PET MPO provides improved differentiations compared to individual physicochemical parameters, among which CNS PET MPO > 3 is preferred for PET ligand

A. Representative antagonist type PET radioligands



B. Representative PAM type PET radioligands

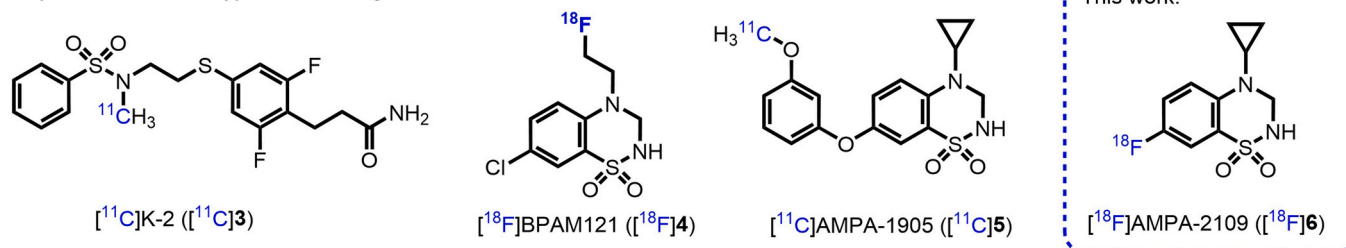


Fig. 1. Representative radioligands for PET imaging of AMPA receptors.

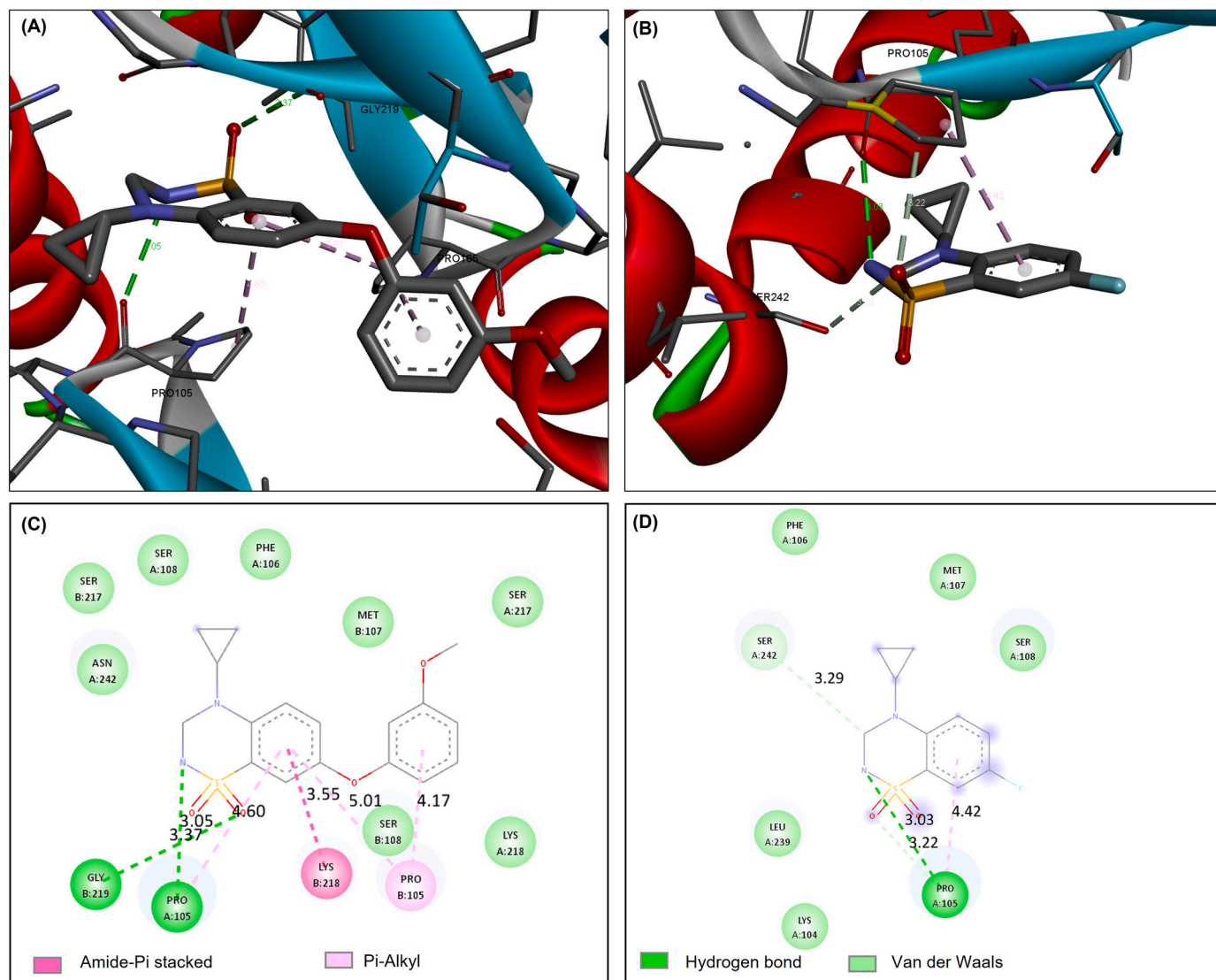


Fig. 2. Comparison structure of GluA2-BLD with AMPA potentiator 5 and 6. (A) The binding mode of molecule 5 (black sticks). BLD residues are show in line representation. Nitrogen atoms are blue, oxygen atoms red, and sulfur atoms yellow. Hydrogen bonds and distances within 5 Å are show as green lines. Van der Waals interaction, Amide-Pi stacked, Pi-Alkyl are showed as light green, purple, and pink respectively. (B) The binding mode of compound 6. (C) The 2D corresponding ligand interaction plot of molecule 5 in BLD, where arrow represents hydrogen bond between sidechain and backbone. (D) The 2D ligand interaction plot of compound 6 in BLD.

development. As shown in Table 1, these compounds had similar CNS MPO scores. Further analysis of the PET ligand properties indicated that compound 6 (CNS PET MPO 5.0), which showed much higher value than that of compound 5 (2.8), would be a better choice for PET tracer

Table 1
Physicochemical properties and MPO calculation of 5 and 6.^a

| Compound 5 | | Compound 6 | |
|------------|-------|--------------------|--------|
| Parameter | Value | Parameter | Value |
| ClogP | 2.42 | ClogP | 1.22 |
| ClogD | 2.42 | ClogD ^b | 1.92 |
| tPSA | 76.25 | tPSA | 57.79 |
| MW | 346.4 | MW | 242.47 |
| HBD | 1 | HBD | 1 |
| pKa | 9.7 | pKa | 9.4 |
| CNS MPO | 4.8 | CNS MPO | 5.1 |
| PET MPO | 2.8 | PET MPO | 5.0 |

^a Data were calculated by ACD/Labs software

^b Data were obtained by the 'shake flask' method.

development.

2.3. Chemistry

We designed and synthesized the precursor for radiolabeling with novel ¹⁸F-labeling methods [20]. Precursor 7 was efficiently synthesized over seven steps from 5-bromo-2-fluoroaniline with 8.9 % overall yield. The characterization of precursor 7 and compound 6 was provided in the Supporting Information.

2.4. Radiochemistry and in vitro metabolic stability study

After successfully obtaining the labeling precursor, we performed the radiolabeling with ¹⁸F to generate PET tracer [¹⁸F]6. As depicted in Fig. 3A, we initially conducted the radiolabeling in anhydrous DMA/*tert*-BuOH at 110 °C with tetraethylammonium bicarbonate (TEAB, 0.6 mg) and Cu(OTf)₂(pyr)₄ (20 mg) for 10 min. Complete deprotection of the Boc group was achieved by the use of HCl (6 N) at 80 °C for 5 min, thus providing [¹⁸F]6 in reasonable decay-corrected radiochemical yield

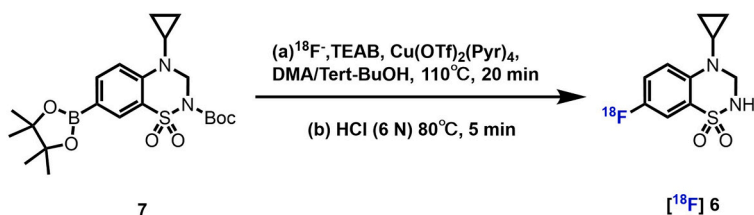
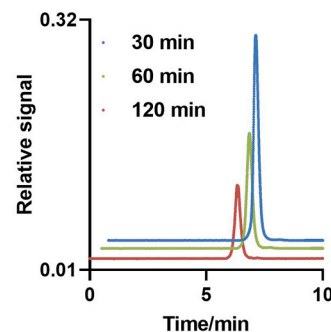
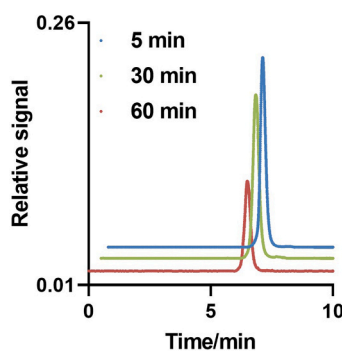
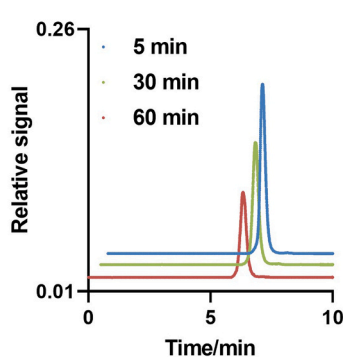
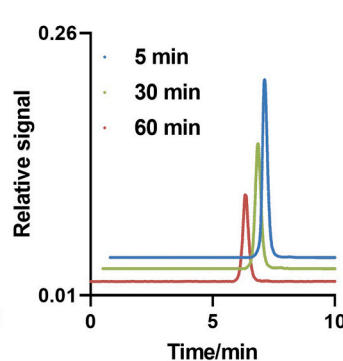
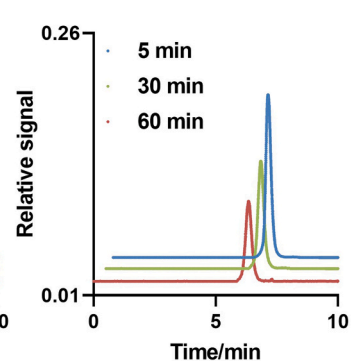
(A) Radiosynthesis of [¹⁸F]6**(B) Formulation Stability****(C) Mouse Serum****(D) Rat Serum****(E) NHP Serum****(F) PBS**

Fig. 3. ¹⁸F labeling of [¹⁸F]6 and stability (in vitro) studies. (A) Radiosynthesis of [¹⁸F]6. (B) Stability of tracer in PBS (containing 5 % ethanol, v/v) (C-E) Stability of tracer in serum of various species (mouse, rat, non-human primate) at three different time point (5, 30, and 60 min). (F) Stability of tracer in PBS as a control group.

(RCY, 12 ± 4 %). At the end of synthesis, [¹⁸F]6 was obtained with excellent radiochemical purity (>99 %) and excellent molar activities (>74 GBq/μmol). In addition, [¹⁸F]6 also showed stability in a formulation composed of saline and 5 % ethanol with no degradation up to 120 min (Fig. 3B). These results translated to serum stability in mouse, rat, NHP serum, and PBS buffer during 60-min study period (Fig. 3C-F).

2.5. PET imaging in rodents

With promising in vitro stability, we next evaluated [¹¹C]5 and [¹⁸F]6 for PET imaging in rodent models. Dynamic PET scans (0–60 min) were acquired following intravenous administration of [¹¹C]5 and [¹⁸F]6 in CD-1 mice (*n* = 3). Representative PET images (coronal and sagittal) are depicted in Fig. 4A. Higher uptake of [¹⁸F]6 than that of [¹¹C]5 was observed in the whole brain. The corresponding whole-brain time-activity curves (TACs) are shown in Fig. 4B. It demonstrated that both tracers [¹¹C]5 and [¹⁸F]6 entered the brain and achieved the highest brain uptake within 2 min, followed by gradual washout for [¹¹C]5 and rapid clearance for [¹⁸F]6. The PET scan demonstrated excellent BBB permeability for [¹⁸F]6 with a peak standard uptake value (SUV_{peak}) of 2.5. Following the quantification analysis of TAC within 60 min, the total uptake of [¹⁸F]6 derived from the area under curve (AUC) was 1.8-fold higher than of [¹¹C]5 in mouse brain (Fig. 4C). These PET imaging results in mice agreed with the prediction of CNS PET MPO analysis. Encouraged by the promising BBB permeability in mice, PET imaging in rats with [¹⁸F]6 and in vivo binding specificity study were carried out for further evaluation. As exhibited in Fig. 4D, [¹⁸F]6 peaked quickly in the rat brain with similar SUV in different brain regions examined. To validate the in vivo binding specificity of [¹⁸F]6 towards AMPA receptors in rats, PET blocking study was also conducted with a dose of K-2 (1 mg/kg, IV) injected 5 min prior to radioligand administration. Pretreatment with K-2, the AMPA specific positive allosteric modulator resulted in 14–16 % reduction of the bound activity in these

brain regions (support information Fig. S1), indicating medium specific binding of [¹⁸F]6 in rodents.

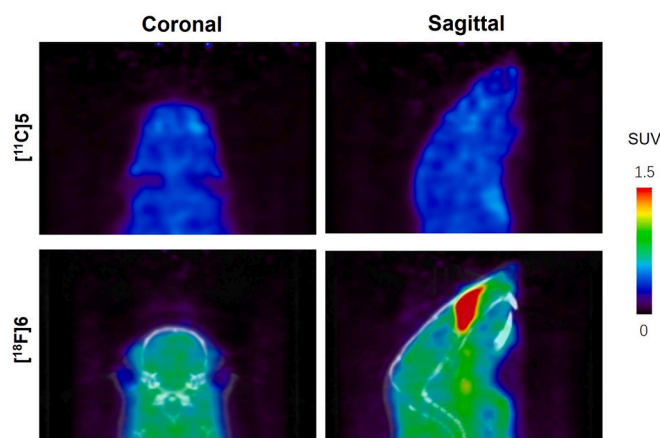
2.6. PET-MRI imaging studies in NHPs

Considering the species variability of AMPA receptors and the difference of high species brain permeability, we then evaluated [¹¹C]5 and [¹⁸F]6 in nonhuman primates to explore brain penetration and regional distribution as a proof-of-concept study. Dynamic PET (0–60 min) data were acquired consecutively on rhesus macaques and representative PET-MRI images (60 min) on the rhesus brain and corresponding TACs for regions of interest (ROI) are illustrated in Fig. 5. To assess the validity of region selectivity, we observed the two radioligands distributed evenly in the same rhesus brain, with no significant differences in ROIs (Fig. 5B & C). It is possible that the two tracers exhibit similar brain region distribution due to the similar backbone structures and low specific binding. The corresponding TACs were then derived from brain uptake and ROI analysis. For all brain regions imaged with [¹¹C]5, the SUV_{max} of ROIs ranged from 1.1 to 1.3 at 5 min (Fig. 5D). On the other hand, [¹⁸F]6 peaked quickly with SUVs ranging from 3.6 to 5.3 at about 3 min (Fig. 5E). Notably, the whole brain AUC of [¹⁸F]6 was much higher than that of [¹⁸F]5 (increased by 36 %), which indicated greater uptake of [¹⁸F]6 (support information Fig. S2). In agreement with PET imaging results in rodents, the brain permeability of [¹⁸F]6 in the high species was consistent with that in mice, which was also in line with our predictions using the MPO analysis.

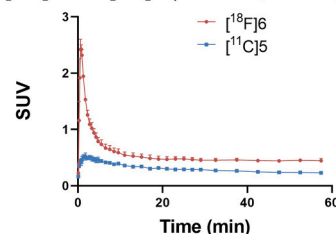
2.7. Ex vivo biodistribution studies of [¹⁸F]6 in rodents

To correlate with our PET imaging results, we sought to evaluate in vivo uptake of [¹⁸F]6 by whole body ex vivo biodistribution. Radioactivity counts were measured in mice and four different time points (5, 15, 30 and 60 min) were selected post injection of [¹⁸F]6. As illustrated

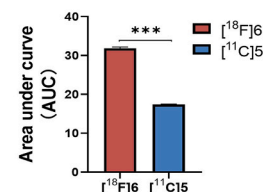
A. Representative PET images of tracer [^{11}C]5 and [^{18}F]6 (0-60 min summed image, mouse)



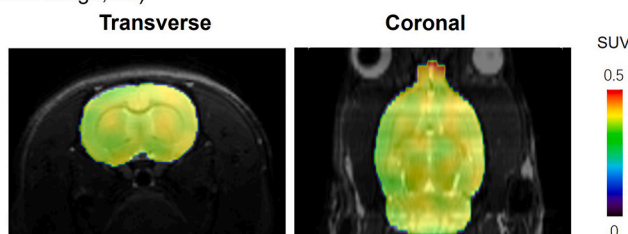
B. Dynamic standard uptake value of [^{11}C]5 and [^{18}F]6 (0-60 min, mouse)



C. Quantification of area under the TACs



D. Representative PET images of tracer [^{11}C]5 and [^{18}F]6 (0-60 min summed image, rat)



E. Dynamic standard uptake value of [^{11}C]5 and [^{18}F]6 (0-60 min, rat)

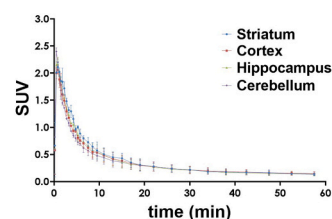


Fig. 4. PET imaging study in rodents. (A) Representative PET images of [^{11}C]5 and [^{18}F]6 in CD-1 mouse brain (averaged 0–60 min) (B) Time activity curves of [^{11}C]5 and [^{18}F]6 in mouse brain. All data are mean \pm SD, $n = 3$. (C) Statistical analysis of the area under curves, t -test, $***p < 0.001$. (D) Representative PET images of [^{18}F]6 in SD rat brain (averaged 0–60 min) (E) Time activity curves of tracer [^{18}F]6 in rat brain. All data are mean \pm SD, $n = 3$.

in Fig. 6, radioactivity uptake was high (>3 %ID/g) in multiple peripheral organs, such as the lung, heart, pancreas, kidney and liver after 5 min injection. Subsequently, relatively slow washout was observed from these organs. Of note, the radioactivity in blood cleared slowly. Furthermore, high renal and hepatic uptake rates (>10 %ID/g) were observed, possibly indicating that the tracer may be excreted through the hepatobiliary and urinary systems. The biodistribution pattern of [^{18}F]6 was consistent with previous data observed from [^{11}C]5.

3. Conclusion

The development of a PET radioligand for the visualization and quantification of AMPA receptors is necessary to better understand the expression and distribution of these receptors in both normal and disease states, as well as to provide a molecular imaging tool for target occupancy studies in drug discovery. Aided by molecular docking and MPO analysis, we have successfully designed and synthesized radioligand [^{18}F]6 in good RCYs ($12 \pm 4\%$) and high radiochemical purity ($>99\%$) by taking advantage of the structural similarity in our previously reported tracer [^{11}C]5. PET imaging results confirmed that radioligand [^{18}F]6 exhibited high brain uptake in the rodent and NHP brain with homogenous distribution and fast kinetics. However, due to the inferior potency of 6, radioligand [^{18}F]6 showed moderate specific binding in the brain. This suggests the need of medicinal chemistry modification to improve binding affinity and washout kinetics. Building upon the findings from the docking study involving compound 6, we posit a hypothesis that enhancing the π -character of the substituent located at position 4 (previously a cyclopropyl group) while carefully modulating the substituent's size to reduce the distance between the molecule and the protein could lead to a significant improvement in the binding affinity of the target molecule. Our work of [^{18}F]6 may serve as a starting

point and offer new insight for the design of novel fluorinated allosteric modulator based AMPA receptor PET tracers for translational PET imaging in higher species.

4. Materials and methods

All animal studies were carried out following the guidelines of Jinan University and Massachusetts General Hospital. All procedures were approved by Laboratory Animal Ethics Committee. The PET imaging with cynomolgus monkey (male, 5 kg, 6 years) was performed at the PET/CT-MRI center of Department of Nuclear Medicine in the First Affiliated Hospital of Jinan University, following the ethical approval of Animal Care and Use Committee of Guangdong Landau Biotechnology Co. Ltd. (Protocol# LDACU 20211210-01). All the procedures with CD-1 mice (female, 22–24 g, 7 weeks) and SD rats (male, 210–230 g, 7 weeks) were performed at Massachusetts General Hospital with approval protocol (#2017N000102). Animals were accommodated on a 12 h light/12 h dark cycle and provided with food and water ad libitum.

4.1. Chemistry

Target compound 6 was purchased from Sigma-Aldrich (Boston, USA) and the corresponding precursor 7 were synthesized according to a previous publication [16]. (See details in the supporting information).

4.2. Molecular docking studies

The published AMPA receptor crystal structures (PDB ID: 4n07 and 5oew) were download from the protein data bank (<https://www.rcsb.org/>). The structures and molecular interactions were analyzed with Discovery Studio Visualizer (v21.1.0.20298).

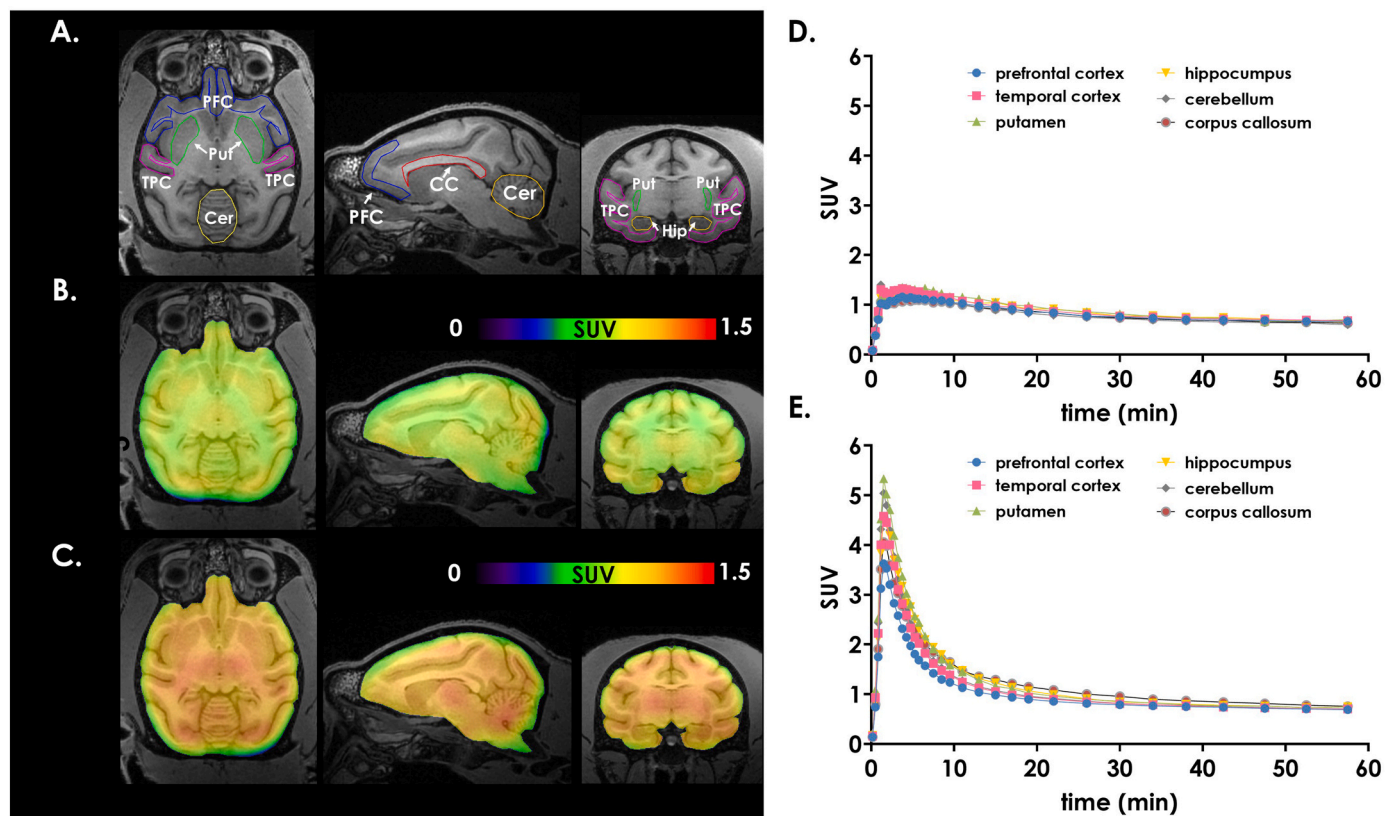


Fig. 5. Representative PET/MRI images of the non-human primate (NHP) brain. (A) Regional assignment was performed based on the acquired MRI image and an overlay was used to define the regions of interest; (B) Representative averaged PET images (0–60 min) under baseline condition with [¹¹C]5; (C) Representative averaged PET images (0–60 min) under baseline condition with [¹⁸F]6; (D) Radioactive time activity curves of [¹¹C]5 in rhesus monkey brain; (E) Radioactive time activity curves of [¹⁸F]6 in rhesus monkey brain.

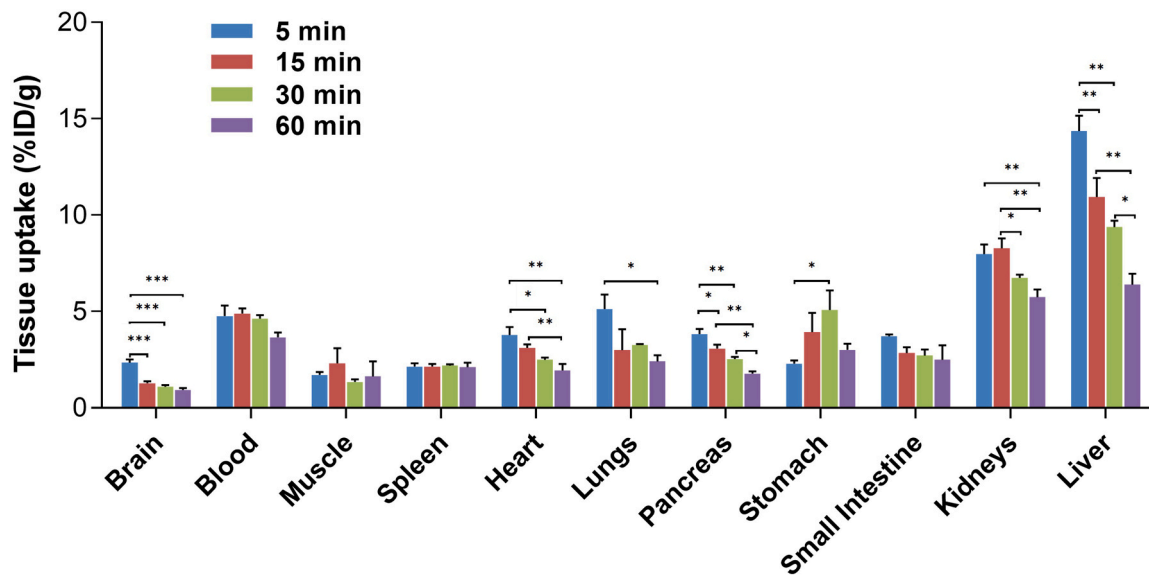


Fig. 6. Whole-body ex vivo biodistribution studies in mice at four different time points (5, 15, 30 and 60 min) post injection of [¹⁸F]6. All data are mean ± SD, n = 3, Asterisks indicate statistical significance. *p < 0.05, **p < 0.01, ***p < 0.001 Data are expressed %ID/g = injected dose per gram of wet tissue.

4.3. CNS PET MPO analysis

The CNS PET MPO was generated using the previously published method [18]. Two candidates' scores were obtained using ACD/laboratories software. Six physicochemical properties commonly considered were calculated in this method, including cLogP, cLogD, MW, tPSA,

HBD, and pKa.

4.4. Radiochemistry

[¹⁸F]F⁻ was trapped on a light QMA cartridge (WAT 023525), and then eluted into a reaction vial with tetraethylammonium bicarbonate

(TEAB, 0.5 mL, 1.2 mg/mL in MeOH). The eluted [^{18}F]F was dried under a stream of nitrogen at 110 °C for 10 min. A solution of labeling precursor **7** (2 mg) and $\text{Cu}(\text{OTf})_2(\text{pyr})_4$ (20 mg) in anhydrous DMA/*tert*-BuOH (300 μL , 2/1, v/v) was added and heated at 110 °C for 20 min. After cooling to 80 °C, 200 μL HCl (6 N) was added to remove the Boc group. The resulting mixture was diluted with HPLC buffer solution and then purified on a semi-preparative HPLC (Phenomenex Luna, 5 μm , C18 column, 10 mm i.d. \times 250 mm) using a mobile phase of $\text{CH}_3\text{CN}/0.1\text{ M AMF}$ (35/65, v/v, pH = 4.5) under the flow rate of 5.0 mL/min. The radioactive fraction corresponding to [^{18}F]6 with a retention time of 21 min was collected and re-formulated with 5 % EtOH in saline. The chemical, radiochemical purity and radiochemical stability were measured by a radioactive analytical HPLC (Phenomenex Luna, 3.5 μm , C18 column, 4.6 \times 150 mm) with an eluent of $\text{CH}_3\text{CN}/\text{AMF}$ (40/60, v/v) at a flow rate of 1.0 mL/min ($t_{\text{R}} = 3\text{ min}$). TEAB = Tetraethylammonium bromide; DMA = N, N-Dimethylacetamide; AMF = Ammonium formate.

4.5. PET imaging in rodents

PET imaging for CD-1 mice was performed on a G4 PET Scanner (Sofie). The mice were anesthetized with 1–2 % (V/V) isoflurane and administered 1.85–3.7 MBq/100 μL of [^{18}F]6 intravenously via the tail vein. Dynamic scans were performed for 60 min and the raw data were reconstructed by using AMIDE software. Regions of interest include the entire brain, hippocampus, cerebral cortex, cerebellum, striatum, thalamus, and pons. $\text{SUV} = (\text{radioactivity per milliliter of tissue/radioactivity injected}) \times \text{bodyweight}$.

4.6. Non-human primate PET-MRI imaging

Compound [^{11}C]5 and [^{18}F]6 were further evaluated in non-human primate PET-MRI studies. The study was performed on a time-of-flight PET/CT scanner (GE Discovery 690 PET/CT Elite). The monkeys were anesthetized with isoflurane and transferred to a PET scanning bed. CT scans were performed before tracer injection for attenuation correction. After intravenous bolus injection, 60 min of three-dimensional dynamic acquisition of brain radioactive signals was performed with 36 frames (6 \times 20 s, 8 \times 30 s, 4 \times 1 min, 5 \times 2 min, 5 \times 4 min, 4 \times 5 min). Magnetic resonance images were acquired from GE 3 T scanner (GE Discovery 750, Milwaukee, USA). Brain images were acquired using T1-weighted echo sequences in three-dimensional space. Brain reconstruction image processing was performed using PMOD (version 4.105) to perform anatomical position registration. Regions of interest (ROIs) were generated manually under the guidance of MRI structural images and summed PET data. SUV of each VOIs and the corresponding time-activity curves (TACs) were generated for statistical analysis.

4.7. Ex vivo biodistribution studies

Ex vivo biodistribution experiments were conducted as previously reported [21]. Briefly, ICR mice (8–10 weeks of age, $n = 16$) were intravenously injected with [^{18}F]6 (3.7 MBq/100 μL) and then sacrificed at different time points (5, 15, 30 and 60 min), respectively. After dissection of the mice, organs and tissues of interest were harvested and weighed. The radioactivity of each organ/tissue was measured with the radioactive gamma counter (2480 WIZARD, Perkin Elmer, Waltham, MA, USA). All data were presented as percent injected dose per gram of wet tissue (%ID/g).

4.8. Statistical analysis

All data are expressed as mean \pm SD. Statistical analysis was performed using an unpaired two-tailed Student's *t*-test and the one-way ANOVA analysis of variance. The differences in SUV between [^{11}C]5 and [^{18}F]6 were evaluated using the paired *t*-test. *P* values less than 0.05

were considered statistically significant.

CRediT authorship contribution statement

All the authors contributed to this manuscript and have approved its final version. S.H.L., L.W., W.H. proposed the study, conceived the project, and guided experiments. J.C. and W.R. wrote the manuscript. S. H.L., H.X. and L.W. modified the paper. J.C., W.R. and Y.H. synthesized the radioligands. J.W., J.R., H.W., G.L., Z.C., L.C., K.L., C.D., Y.L. carried out the experiments. J.C., W.R., J.W., N.H.E., W.S., and A.H. analyzed the data.

Declaration of Competing Interest

The authors have no conflicts of interest to declare.

Acknowledgements

We gratefully acknowledge the support of K.C. Wong Education Foundation (China). This work in our group was supported by the National Natural Science Foundation of China (No. 82001881, 82071974, China), Guangzhou Science and Technology Program (No. 202206010106, China), Guangdong Special Program for Science and Technology Innovation (No. 2022A0505050042, China), and the Clinical Frontier Technology Program of the First Affiliated Hospital of Jinan University (No. JNU1AFCFTP-2022-a01214, China).

Appendix A. Supporting information

Supplementary data associated with this article can be found in the online version at [doi:10.1016/j.biopha.2023.115842](https://doi.org/10.1016/j.biopha.2023.115842).

References

- [1] O.R. Buonarati, E.A. Hammes, J.F. Watson, I.H. Greger, J.W. Hell, Mechanisms of postsynaptic localization of AMPA-type glutamate receptors and their regulation during long-term potentiation, *Sci. Signal* 12 (2019) 562.
- [2] D.W. Allison, V.I. Gelfand, I. Spector, A.M. Craig, Role of actin in anchoring postsynaptic receptors in cultured hippocampal neurons: differential attachment of NMDA versus AMPA receptors, *J. Neurosci.* 18 (7) (1998) 2423–2436.
- [3] T.E. Chater, Y. Goda, The role of AMPA receptors in postsynaptic mechanisms of synaptic plasticity, *Front. Cell Neurosci.* 8 (2014) 401.
- [4] D.S. Younger, Autoimmune encephalitis, *Neurol. Clin.* 37 (2) (2019) 359–381.
- [5] L. Volk, S.L. Chiu, K. Sharma, R.L. Huganir, Glutamate synapses in human cognitive disorders, *Annu. Rev. Neurosci.* 38 (2015) 127–149.
- [6] B. Pirotte, P. Francotte, E. Goffin, P. Fraikin, L. Danober, B. Lesur, I. Botez, D. H. Caignard, P. Lestage, P. de Tullio, Ring-fused thiadiazines as core structures for the development of potent AMPA receptor potentiators, *Curr. Med. Chem.* 17 (30) (2010) 3575–3582.
- [7] L.R. Watterson, M.F. Olive, Are AMPA receptor positive allosteric modulators potential pharmacotherapeutics for addiction? *Pharmaceuticals (Basel)* 7 (1) (2013) 29–45.
- [8] M.E. Phelps, Positron emission tomography provides molecular imaging of biological processes, *Proc. Natl. Acad. Sci. USA* 97 (16) (2000) 9226–9233.
- [9] T. Fuchigami, M. Nakayama, S. Yoshida, Development of PET and SPECT probes for glutamate receptors, *Sci. World J.* 2015 (2015), 716514.
- [10] H.G. Lee, P.J. Milner, M.S. Placzek, S.L. Buchwald, J.M. Hooker, Virtually instantaneous, room-temperature [(11)C]-cyanation using biaryl phosphine Pd(0) complexes, *J. Am. Chem. Soc.* 137 (2) (2015) 648–651.
- [11] K. Takahata, Y. Kimura, C. Seki, M. Tokunaga, M. Ichise, K. Kawamura, M. Ono, S. Kitamura, M. Kubota, S. Moriguchi, T. Ishii, Y. Takado, F. Niwa, H. Endo, T. Nagashima, Y. Ikoma, M.R. Zhang, T. Suhara, M. Higuchi, A human PET study of [(11)C]HMS011, a potential radioligand for AMPA receptors, *EJNMMI Res.* 7 (1) (2017) 63.
- [12] N. Oi, M. Tokunaga, M. Suzuki, Y. Nagai, Y. Nakatani, N. Yamamoto, J. Maeda, T. Minamimoto, M.R. Zhang, T. Suhara, M. Higuchi, Development of novel PET probes for central 2-amino-3-(3-hydroxy-5-methyl-4-isoxazolyl)propionic acid receptors, *J. Med. Chem.* 58 (21) (2015) 8444–8462.
- [13] T. Arisawa, T. Miyazaki, W. Ota, A. Sano, K. Suyama, Y. Takada, T. Takahashi, [(11)C]K-2 image with positron emission tomography represents cell surface AMPA receptors, *Neurosci. Res.* 173 (2021) 106–113.
- [14] A. Manos-Turvey, G. Becker, P. Francotte, M.E. Serrano, A. Luxen, B. Pirotte, A. Plenevaux, C. Lemaire, Fully automated synthesis and evaluation of [(18)F]BPAMI21: potential of an AMPA receptor positive allosteric modulator as PET radiotracer, *ChemMedChem* 14 (7) (2019) 788–795.

- [15] E. Goffin, T. Drapier, A.P. Larsen, P. Geubelle, C.P. Ptak, S. Laulumaa, K. Rovinskaja, J. Gilissen, P. Tullio, L. Olsen, K. Frydenvang, B. Pirotte, J. Hanson, R.E. Oswald, J.S. Kastrop, P. Francotte, 7-Phenoxy-substituted 3,4-dihydro-2H-1,2,4-benzothiadiazine 1,1-dioxides as positive allosteric modulators of α -amino-3-hydroxy-5-methyl-4-isoxazolepropionic acid (AMPA) receptors with nanomolar potency, *J. Med. Chem.* 61 (1) (2018) 251–264.
- [16] J. Chen, J. Gan, J. Sun, Z. Chen, H. Fu, J. Rong, X. Deng, J. Shang, J. Gong, T. Shao, L. Collier, L. Wang, H. Xu, S.H. Liang, Radiosynthesis and preliminary evaluation of (11)C-labeled 4-cyclopropyl-7-(3-methoxyphenoxy)-3,4-dihydro-2H-benzo[e][1,2,4]thiadiazine 1,1-dioxide for PET imaging AMPA receptors, *Tetrahedron Lett.* 61 (12) (2020).
- [17] A.B. Norholm, P. Francotte, L. Olsen, C. Krintel, K. Frydenvang, E. Goffin, S. Challal, L. Danober, I. Botez-Pop, P. Lestage, B. Pirotte, J.S. Kastrop, Synthesis, pharmacological and structural characterization, and thermodynamic aspects of GluA2-positive allosteric modulators with a 3,4-dihydro-2H-1,2,4-benzothiadiazine 1,1-dioxide scaffold, *J. Med. Chem.* 56 (21) (2013) 8736–8745.
- [18] L. Zhang, A. Villalobos, Strategies to facilitate the discovery of novel CNS PET ligands, *EJNMMI Radiopharm. Chem.* 1 (1) (2017) 13.
- [19] T.T. Wager, X. Hou, P.R. Verhoest, A. Villalobos, Central nervous system multiparameter optimization desirability: application in drug discovery, *ACS Chem. Neurosci.* 7 (6) (2016) 767–775.
- [20] X. Deng, J. Rong, L. Wang, N. Vasdev, L. Zhang, L. Josephson, S.H. Liang, Chemistry for positron emission tomography: recent advances in (11) C-, (18) F-, (13) N-, and (15) O-labeling reactions, *Angew. Chem. Int. Ed. Engl.* 58 (9) (2019) 2580–2605.
- [21] Z. Chen, W. Mori, J. Rong, M.A. Schafroth, T. Shao, R.S. Van, D. Ogasawara, T. Yamasaki, A. Hiraishi, A. Hatori, J. Chen, Y. Zhang, K. Hu, M. Fujinaga, J. Sun, Q. Yu, T.L. Collier, Y. Shao, B.F. Cravatt, L. Josephson, M.R. Zhang, S.H. Liang, Development of a highly-specific (18)F-labeled irreversible positron emission tomography tracer for monoacylglycerol lipase mapping, *Acta Pharm. Sin. B* 11 (6) (2021) 1686–1695.